

Ca:Mg:Zn:CO₃ and Ca:Mg:CO₃ tri- and bi-elemental carbonate microparticles for novel injectable self-gelling hydrogel-microparticle composites for tissue regeneration

Timothy E.L. Douglas^{1,2*}, Katarzyna Sobczyk³, Agata Łapa³, Katarzyna Włodarczyk⁴, Gilles Brackman⁵, Irina Vidiyasheva⁶, Katarzyna Reczyńska³, Krzysztof Pietryga³, David Schaubroeck⁷, Vitaliy Bliznuk⁸, Pascal Van Der Voort⁹, Heidi A. Declercq¹⁰, Jan Van den Bulcke¹¹, Sangram Keshari Samal^{12,13}, Dmitry Khalenkov¹, Bogdan V. Parakhonskiy^{1,14}, Joris Van Acker¹¹, Tom Coenye⁵, Małgorzata Lewandowska-Szumiel⁴, Elżbieta Pamuła³, Andre G. Skirtach^{1,13}

¹Department of Molecular Biotechnology, Ghent University, Coupure Links 653, 9000 Gent, Belgium, ²Engineering Department, Lancaster University, United Kingdom, ³Department of Biomaterials, Al. Mickiewicza 30, 30-059, Faculty of Materials Science and Ceramics, AGH University of Science and Technology, Kraków, Poland, ⁴Tissue Engineering Laboratory, Department of Histology and Embryology, Medical University of Warsaw, Chałubińskiego 5, 02-004 Warsaw, Poland, ⁵Laboratory of Pharmaceutical Microbiology (LPM), Dept. Pharmaceutical Analysis, Ghent University, Belgium, ⁶Institute of Nanostructures and Biosystems, Cell engineering Department, Saratov State University, Russian Federation, ⁷Center for Microsystems Technology (CMST), imec and Ghent University, Technologiepark 914a, 9052 Ghent, Belgium, ⁸Department of Material Science & Engineering, Tech Lane Ghent Science Park – Campus A, Technologiepark 903, 9052 Zwijnaarde, Belgium, ⁹Department of Inorganic Chemistry, Center for Ordered Materials Organometallics and Catalysis (COMOC), Ghent University, Krijgslaan, 281 S3, 9000, Ghent Belgium, ¹⁰Department of Basic Medical Science – Tissue Engineering Group, Ghent University, De Pintelaan 185 (6B3), 9000 Ghent, Belgium, ¹¹UGCT-Woodlab, Laboratory of Wood Technology, Department of Forest and Water Management, Ghent University, Belgium, ¹²Laboratory of General Biochemistry and Physical Pharmacy, Ghent University,

Ottergemsesteenweg 460, 9000 Ghent, Belgium, ¹³Centre for Nano- and Biophotonics, Ghent University, Ottergemsesteenweg 460, 9000 Ghent, Belgium, ¹⁴Shubnikov Institute of Crystallography, RAS, Moscow, Russian Federation

*Corresponding Author. Email: t.douglas@lancaster.ac.uk

Formatted: English (United States)

Keywords: hydrogel, gellan gum, carbonate, injectable material, magnesium, zinc, composite

Abstract

Injectable composites for tissue regeneration can be developed by dispersion of inorganic microparticles and cells in a hydrogel phase. In this study, multifunctional carbonate microparticles containing different amounts of calcium, magnesium and zinc were mixed with solutions of gellan gum (GG), an anionic polysaccharide, to form injectable hydrogel-microparticle composites, containing Zn, Ca and Mg. Zn and Ca were incorporated into microparticle preparations to a greater extent than Mg. Microparticle groups were heterogeneous and contained microparticles of differing shape and elemental composition. Zn-rich microparticles were “star shaped” and appeared to consist of small crystallites, while Zn-poor, Ca- and Mg-rich microparticles were irregular in shape and appeared to contain larger crystallites. Zn-free microparticle groups exhibited the best cytocompatibility and, unexpectedly, Zn-free composites showed the highest antibacterial activity towards Methicilin-resistant *Staphylococcus aureus* (MRSA). Composites containing Zn-free microparticles were cytocompatible and therefore appear most suitable for applications as an injectable biomaterial. This study proves the principle of creating bi- and tri-elemental microparticles to induce the gelation of GG to create injectable hydrogel-microparticle composites.

1. Introduction

Hydrogels, or three dimensional polymer networks containing entrapped water, represent an important class of materials for tissue regeneration. They have been enriched with pre-formed inorganic particles to improve their suitability for bone regeneration (Gkioni et al., 2010). One such hydrogel material is gellan gum (GG) (Douglas et al., 2014b, Gorodzha et al., 2016), which is an anionic polysaccharide, and can be crosslinked with divalent ions such as Ca^{2+} , Mg^{2+} and Zn^{2+} to form hydrogels.

Certain organic particles, e.g. bioactive glasses and calcium carbonate (CaCO_3), can release divalent ions. Particles dispersed in anionic polymer solution can release divalent ions slowly, leading to homogeneous hydrogel [formation](#), a concept known as “internal gelation” (Chan et al., 2002). In the case of CaCO_3 , [Ca²⁺ release from the particles may be insufficient to induce hydrogel gelation \(Douglas et al., 2016b\). At pH =7 particles are rather stable and the ion release rate is very slow and strongly depends on crystallographic stability. For example, CaCO₃ in the vaterite polymorph state releases ions rather more quickly than the more stable calcite polymorph \(Parakhonskiy et al., 2013\) But at pH lower than 6.5, CaCO₃ can release ions faster which can lead to total mineral dissolution \(Svenskaya et al., 2013\). Hence,](#) acidifiers such as glucono-delta-lactone (GDL) are necessary to promote dissolution and ion release (Kuo and Ma, 2001). Alternatively, the polymer solution needs to be at an acidic pH (Moreira et al., 2014).

[CaCO₃ has also been widely and successfully applied in bone regeneration \(Viateau et al., 2013\) and for implant surface modification \(Savelyeva et al., 2017\). CaCO₃ microparticles have also been investigated as delivery vehicles for biologically active substances \(Donatan et al., 2016, Svenskaya et al., 2016\).](#)

[Recently, many publications have appeared on the enrichment of inorganic materials with magnesium for bone regeneration, where it has been shown that these materials promote](#)

mouse osteoblast cell proliferation *in vitro* (Douglas et al., 2014c) and bone regeneration *in vivo* (Landi et al., 2006, Zhao et al., 2012). Zinc incorporation has also been shown to endow antibacterial properties to a variety of biomaterials (Douglas et al., 2015, Thian et al., 2013).

However, magnesium and zinc enrichment of carbonate-based biomaterials for bone regeneration remains unexplored.

Hence, the addition of inorganic carbonate particles containing magnesium and zinc to GG solution would serve a triple function. Firstly, the addition of microparticles would induce homogenous gelation by slow release of the divalent ions. Secondly, the presence of the inorganic particles would increase the suitability for applications in bone regeneration. Thirdly, the presence of magnesium and zinc would be expected to lead to an increase in cell number and endow antibacterial activity, respectively.

In this work, self-gelling hydrogel-particle composites were generated by addition of carbonate microparticles containing magnesium, calcium and zinc to the GG solution. This approach was used in previous work to cause formation of self-gelling composites of GG and bioactive glass particles (Douglas et al., 2014b, Gorodzha et al., 2016). Previous work on carbonate microparticles containing magnesium and calcium revealed that increasing Mg content of microparticles increased amorphicity, which presumably led to higher ion release (Douglas et al., 2016b). One of the advantages of this approach is the avoidance of acidifiers such as GDL or an acidic pH of the polymer solution to cause microparticle dissolution, ion release and hydrogel formation.

Tri-elemental or bi-elemental carbonate microparticles were preformed by mixing a solution containing Ca^{2+} , Mg^{2+} and Zn^{2+} ions or Ca^{2+} and Mg^{2+} ions with another solution containing CO_3^{2-} ions. Three different $\text{Ca}^{2+}:\text{Mg}^{2+}:\text{Zn}^{2+}$ concentration ratios were compared.

The effect of $\text{Ca}^{2+}:\text{Mg}^{2+}:\text{Zn}^{2+}$ concentration ratio on particle composition was evaluated.

Elemental composition was determined using X-ray fluorescence (XRF). Attenuated total

reflectance Fourier-transform infrared spectroscopy (ATR-FTIR), Raman spectroscopy, transmission electron microscopy (TEM), elemental mapping based on energy-dispersive X-ray spectroscopy (EDS), selected area electron diffraction (SAED), scanning electron microscopy (SEM), [X-Ray diffraction \(XRD\)](#), laser diffraction and thermogravimetric analysis (TGA) were also carried out. Cytocompatibility of microparticles was tested by the standard [alamarBlue®](#) assay.

After addition of particles to the GG solution, the speed of gelation was evaluated by rheometry. Composites were characterized biologically by cytocompatibility tests to evaluate osteoblast-like cell growth on, under and in the composites. Antibacterial activity against Methicilin-resistant *Staphylococcus aureus* (MRSA) was also tested.

As mentioned above, enrichment of calcium carbonate biomaterials for bone contact with metal ions other than Ca^{2+} (e.g. Mg^{2+} , Zn^{2+}) has not been well explored. This study aims to fill the gaps in the scientific literature and elucidate the physicochemical and biological effects of incorporation of magnesium and zinc into carbonate microparticles and the effect of such particles on hydrogel formation.

2. Materials and Methods

2.1 Materials

All materials, including GG (Gelzan™ CM, Product no. G1910, “Low-Acyl”, molecular weight 200-300 kD), were obtained from Sigma-Aldrich, unless stated otherwise.

2.2 Production of microparticles

Three groups of microparticles containing different concentrations of CaCl_2 , MgCl_2 and ZnCl_2 were obtained. These were denoted as groups 1, 2 and 3, respectively (see Table 1).

<u>Microparticle group</u>	CaCl₂	MgCl₂	ZnCl₂
1	0.167 M	0.125 M	0.042 M
2	0.167 M	0.083 M	0.083 M
3	0.167 M	0.167 M	0.000 M

Table 1. Concentrations of solutions used to produce microparticle groups 1, 2 and 3

Briefly, 4 ml of a solution containing CaCl₂, MgCl₂ and/or ZnCl₂ (see Table 1) was mixed with 4 ml Na₂CO₃ solution (0.333 M) using a magnetic stirrer. The mixture was stirred for 1 min at room temperature at a speed of 1000 rpm using a magnetic stirrer, leading to the formation of microparticles in the suspension. Next, the solution was poured into four 2 ml Eppendorf tubes and centrifuged for 2 min, at 4°C, at the speed of 9500 rpm. Afterwards, 1 ml of the supernatant was removed and 1 ml of distilled water was added. Eppendorf tubes were shaken carefully using a vortex, and were again centrifuged for 5 min, at 4°C, with the speed of 2 000 rpm. This process allowed removal of unbound Na⁺ and Cl⁻ ions. Subsequently, the whole supernatant was removed and a precipitate of the microparticles was transferred onto a Petri dish and dried in an oven at 60°C for 24 h.

Dried samples were ground in a mortar, sterilized by autoclaving at 121°C for 15 min, dried in an oven for 1 h at 37°C and analyzed.

2.3 Physicochemical and morphological characterization of microparticles: ATR-FTIR, Raman, SEM, TEM, SAED, XRD, XRF, Laser diffraction

A FTIR spectrometer from Perkin Elmer type Spectrum BX in ATR mode (attenuated total reflectance) was used to obtain infrared spectra of the dried microparticles. The spectra were recorded over the wavenumber range 4000-550 cm⁻¹ with a resolution of 4 cm⁻¹.

For Raman analysis, 5 μl of a microparticle suspension in water (2.5 % (w/v)) was placed on a CaF plate and scanned with a WITec Alpha300R+ confocal Raman microscope. The system was equipped with a 785 nm excitation diode laser (Toptica) and an UHTS 300 spectrometer with a -60 °C cooled CCD camera (ANDOR iDus 401 BR-DD). 100x/0.9 NA Nikon objective was used. Spectra were acquired with an integration time of 2s and laser power of 120 mW (measured before the objective). Lateral resolution was 0.5 μm per pixel. Background subtraction was performed in R with in-house built scripts.

SEM analysis of the microparticles was performed using a Jeol JSM-5600 instrument. The instrument was used in the secondary electron mode (SEI). The SEM instrument was equipped with an electron microprobe JED 2300. Prior to this analysis, dried microparticles were coated with a thin layer of gold (ca. 20 nm), using a plasma magnetron sputter coater.

The EDS technique provided elemental analysis and chemical characterization of microparticles. The method used standardless EDAX ZAF quantification with the SUTW-Sapphire detector. For this purpose, a NOVA NANOSEM 200 instrument was used. Micrographs were recorded at 5 and 10 kV acceleration voltage with magnifications ranging from 350x to 10000x. Prior to analysis, microparticles were carbon sputter coated.

Transmission electron microscopy (TEM) analysis was performed using a JEM-2200FS FEG (Jeol) instrument operated at 200 kV. Conventional TEM brightfield (TEM BF), selected area electron diffraction (SAED) and scanning transmission (STEM) modes were used in this work. An in-column omega filter was used to diminish chromatic aberration caused by inelastic scattering of primary electrons in thick areas of the sample. EDS spectrometry was used in combination with STEM mode to measure chemical compositions and produce elemental mappings of the microparticle aggregates.

[XRD measurements were performed as described previously \(Douglas et al., 2016b\). Briefly, a Thermo Scientific™ ARL™ X'TRA Powder Diffractometer was used \(settings: 40 kV, 30](#)

mA, slits used: 0.6 and 1 at source side, 0.6 and 0.2 at detector side, continuous scan mode, 2Theta range 10-50, step size = 0.02 degrees, scan rate 1.2 s/step). Post processing data analysis was performed with Highscore plus software by PANalytical B.V. (Netherlands). Phase content analysis was performed by the semiquantative Rietveld method. Theoretical spectra of calcite, vaterite, sodium chloride, calcium magnesium carbonate (dolomite) and aragonite were taken from the works of Sitepu (Sitepu, 2009), Le Bail et al. (Le Bail et al., 2011), Strel'tsov et al. (Strel'tsov et al., 1987), Reeder and Markgraf (Reeder and Markgraf, 1986) and Jarosch and Heger (Jarosch and Heger, 1986), respectively.

XRF measurements were performed on a NEX CG from Rigaku using a Mo-X-ray source.

For TGA a Sensys evo TG-DSC was used in coupled mode, recording the mass loss and calorimetry simultaneously. Dried microparticles were heated in the temperature range between 30°C and 800°C in an oxygen atmosphere with a heating rate of 10 K/min. The results were analyzed with the Thermal Analysis Software of Calisto.

The microparticle size distribution was examined by a laser diffraction method. Test was performed using Mastersizer 2000 with Hydro S detector (Malvern Instruments). Before the experiment, a suspension was prepared by ultrasound mixing of microparticle with water and a dispersive substrate (Dispex).

2.4 Cytocompatibility testing of microparticles using fibroblasts

Normal human dermal fibroblasts (NHDF) were provided by the Department of Molecular Biotechnology (Ghent University). Cells were used in passage of 2 or 3. All cells were plated separately in tissue culture flasks and cultivated in Dulbecco's Modified Eagle Medium (DMEM, Sigma-Aldrich), containing 10% fetal bovine serum (FBS, Hyclone), 2 mM of L-glutamine (Sigma-Aldrich) and 1% antibiotic antifungal cocktail (Sigma-Aldrich). The media were replaced every 3 days, and cells were maintained in a humidified incubator at 37°C with

5% CO₂. The cell culture with 80% confluence was harvested using 0.25% trypsin (Life technologies) and counted with a hemocytometer.

Cell viability: NHDF cells were seeded into a 12-well cell-culture plate at a cell density of 10⁵/well. After their 24 h cultivation, 200 µl of a 2.5 % (w/v) suspension of microparticle groups 1, 2, or 3 were added into the plate in triplicate and incubated overnight at 37 °C under 5% CO₂. 1 ml of fresh medium and 100 µL of fluorescence dye [AlamarBlue®](#) (Sigma-Aldrich) were added to each well. Intensity was measured by spectrophotometry (Gemini XPS Microplate Reader, Molecular Devices) by absorbance measurements at 560 nm and 635 nm after 4 h of incubation. All materials were sterilized by autoclaving at 121°C for 15 min. The percentage difference between treated and control cells was calculated using equation (1).

$$\% \text{ difference} = \frac{\text{FI 635 of test agent}}{\text{FI 635 of untreated control}} \times 100 \quad (1)$$

where FI 635 = Fluorescence Intensity at 635 nm (560 nm excitation). [For all sample groups, n = 3.](#)

2.5 Preparation of Gellan Gum (GG) solution, formation of hydrogel-microparticle composites and rheometric testing

Sterile GG solution was prepared as described previously (Douglas et al., 2014b). 0.8 ml liquid of GG solution previously heated up to 60°C, 0.02 g of dry microparticles and 0.2 ml distilled H₂O was mixed in Eppendorf tubes using an ultrasonic mixer (Figure S1). Subsequently, all of the Eppendorf tubes were placed in a water bath [at 50°C. This was to help to hinder premature gelation due to cooling.](#) New, empty Eppendorf tubes were placed in a beaker with water heated up to 37°C, [also to hinder premature gelation.](#) To obtain composites, the GG-microparticle suspension was taken up into a syringe and injected into

empty Eppendorf tubes in the beaker. The composites were then incubated at 37°C for 20-30 min to complete the gelation process.

Gelation speed was investigated by performing rheometrical measurements with an AR1000N Rheometer (TA Instruments). All experiments were performed at 37° C at the strain of 0.1% and frequency 1 Hz using a plate-cone setup with a stainless steel plate and an acrylic cone of 4 cm diameter.

2.6 Antibacterial testing of hydrogel-microparticle composites

Antibacterial properties were evaluated using Methicilin-resistant *Staphylococcus aureus* (MRSA) as in previous work (Douglas et al., 2016a, Douglas et al., 2014b, Douglas et al., 2015). Briefly, hydrogel-microparticle composites of volume 0.8 ml were submerged with a silicone disc in 1 ml Müller-Hinton broth containing 10⁴ Colony Forming Units (CFU) of MRSA strain Mu50. After 24 h incubation at 37°C, composites and medium were removed and discs were washed with physiological saline to remove non-adhered bacteria. Discs were collected and the number of CFU per silicone discs was determined by plating. Silicone discs without added hydrogels served as a control. Microparticle-free GG hydrogels were formed by heating 0.64 ml 0.875% (w/v) GG solution to 70°C, adding 0.16 ml 0.15% (w/v) CaCl₂ and cooling to room temperature. GG solution was heated to 70°C to prevent premature gelation after CaCl₂ addition. For all sample groups, n = 3.

2.7 Cytocompatibility testing of hydrogel-microparticle composites

Preliminary cytocompatibility observations were performed in order to verify if MC3T3-E1 osteoblast-like cell viability in the potentially injectable hydrogel-based system is comparable to that obtained in a routine observation of cells in contact with the hydrogel. For this purpose, three different combinations were tried. In the first combination, cells were seeded onto the surface of hydrogel-microparticle composites (Combination 1). In the second

Field Code Changed

combination, cells were seeded on the bottom of the well, and after 4 hours of incubation, when all cells were adherent, hydrogels were formed on top of the cell layer (Combination 2).

In the third combination, cells were suspended in the composite which mimics the potentially injectable system (Combination 3). In all the cases MC3T3-E1 osteoblast-like cells were used to seed the composites and the culture was performed in 24-well plates. The volume of the hydrogel-microparticle composites was 0.5 ml. 1 ml cell culture medium was added. Cells were cultured for 7 days in α -MEM medium supplemented with 10% foetal bovine serum, 1% L-glutamine and 1% antibiotic. Live/dead staining was performed after 1 day and 7 days.

Growth medium was removed and cells were washed with Dulbecco's phosphate-buffered saline (D-PBS). Working solution (2 μ l calcein-AM and 2 μ l propidium iodide/ 1 ml D-PBS), prepared according to the protocol, was added directly to cells. Samples were incubated for 10 minutes in the dark at room temperature. The labeled cells were viewed under the fluorescence microscope (Olympus IX 81). Viable cells were stained with calcein-AM (λ_{ex} 490 nm, λ_{em} 515 nm, green fluorescence) and dead cells were stained with propidium iodide (λ_{ex} 535 nm, λ_{em} 617 nm, red fluorescence).

Calcein-AM (acetoxymethyl ester of calcein) is highly lipophilic and cell membrane permeable. In viable cells the nonfluorescent calcein-AM is hydrolyzed to a green-fluorescent calcein by intracellular esterases. Alternatively, propidium iodide penetrates only through a damaged membrane of dead cells and binds to double stranded DNA in the cell to emit red fluorescence.

3. Results

3.1 Physicochemical characterization of microparticles

SEM analysis (Figure 1) showed that microparticle group 1 contained two different types of microparticles, namely spherical ones of different diameters (under 10 μm), and smaller, more elongated ones. Images of microparticles of group 2 revealed both spherical, smooth microparticles and round microparticles with rough surfaces. Microparticles in group 3 were more irregular in shape, but some spherical microparticles could be also observed. SEM demonstrated also that sizes of microparticles were all in micrometer sized, but microparticles in group 1 were considerably smaller than those in groups 2 and 3.

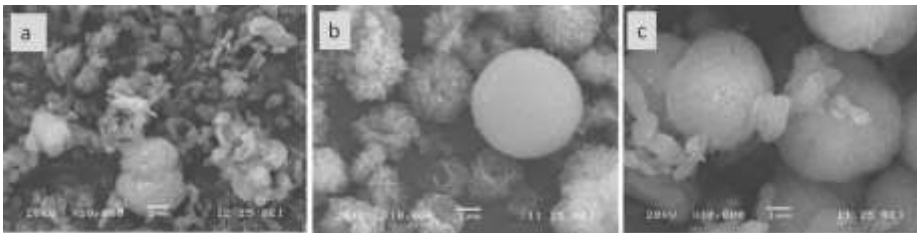


Figure 1. SEM images of microparticle groups 1 (a), 2 (b) and 3 (c), at a magnification of 10 000x

EDS analysis revealed semi-quantitative information about the elemental composition of the different microparticle groups (see Figure S2). As expected, Zn was detected in groups 1 and 2 but was absent in group 3. The occurrence of the elements Na, K and Cl is probably due to a contamination during sample handling.

The chemical composition of microparticles determined by XRF is presented in Table 2. It can be noted that the most predominant elements in all of the microparticle groups (1, 2 and 3) were Ca and Mg. The amount of Zn was high in groups 1 and 2, but in group 3 the content

of Zn was below the detection limit. In group 2, the amounts of Ca and Zn were comparable. In group 3, considerably more calcium was present than magnesium, despite the equimolar concentrations used during microparticle preparation (Table 1). In groups 1 and 2, more Zn was incorporated proportionally than Mg.

Microparticle group	Mg (mass%)	Ca (mass%)	Zn (mass%)	<u>Other elements (mass%)</u>
1	2.51	12.90	7.76	<u>76.83</u>
2	1.81	9.59	11.50	<u>77.10</u>
3	4.89	15.60	0.00	<u>79.51</u>

Table 2. XRF analysis of microparticle groups 1, 2 and 3

Laser diffraction analysis confirmed that the diameters of most microparticles in all three groups (1, 2 and 3) were in the range of 1-3 μm (see Figure S3).

Results of TEM analysis and EDS-based elemental mapping are shown in Figure 2 and Figures S4, S5 and S6, respectively. In microparticle groups 1 and 2, different microparticle types were observed with different elemental compositions. Microparticle groups 1 and 2 both contained both “star shaped” deposits which were Zn- and Mg-rich and Ca-poor and irregularly shaped deposits which contained mainly Ca. In microparticle group 3, only the irregularly shaped deposits which contained mainly Ca were present.

Results of TEM and SEAD analysis of the microparticles are presented in Figure 2. “Star shaped” microparticles in groups 1 and 2 showed defined diffraction rings consisting of small dots, suggesting the presence of small crystallites. Irregular Ca-rich microparticles in groups 1, 2 and 3 also showed diffraction rings with larger dots. This suggested the presence of larger crystallites.

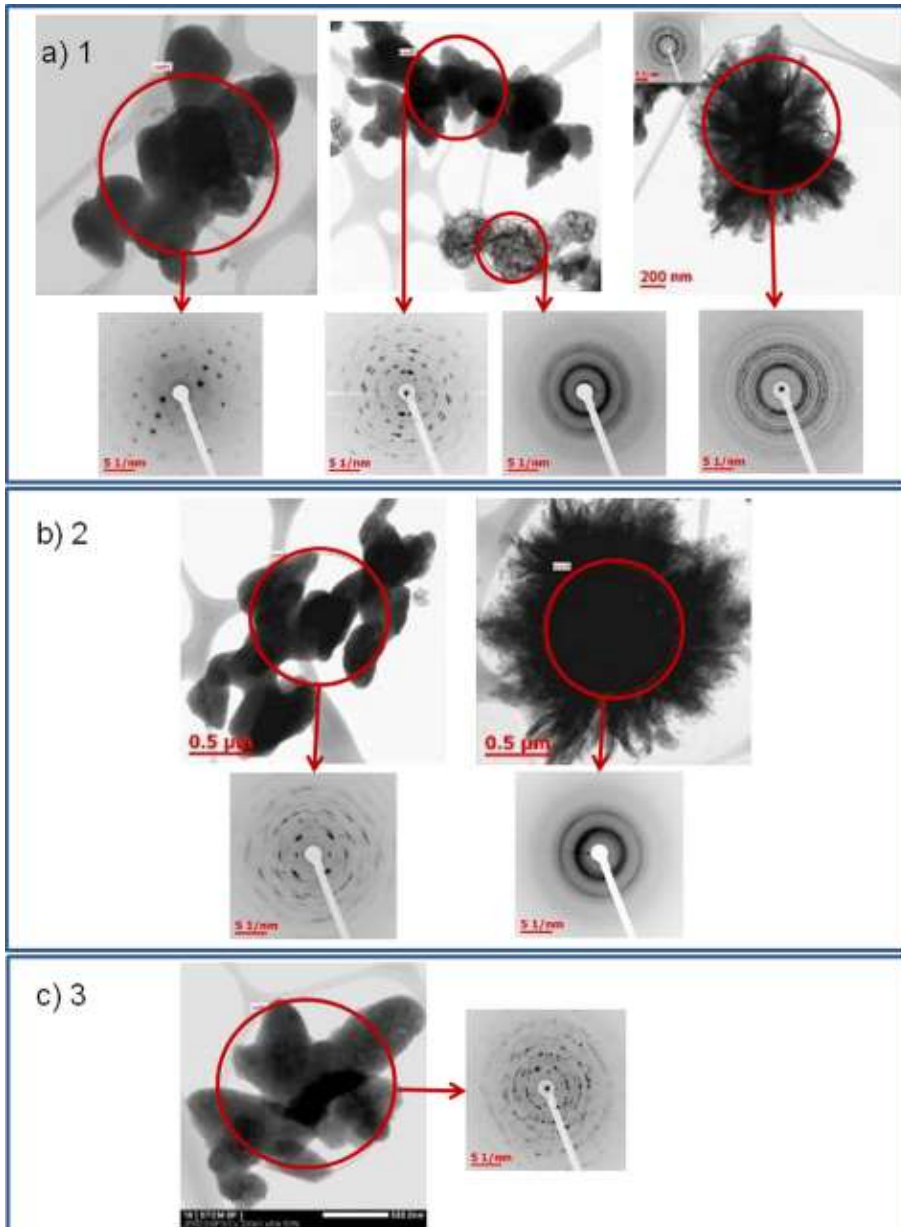


Figure 2. TEM images of microparticle groups 1 (a, top), 2 (b, middle) and 3 (c, bottom) and associated SAED patterns.

Results of XRD analysis of the microparticles are presented in Figure 3. Calcium magnesium carbonate, NaCl, some vaterite and aragonite were detected. No peaks corresponding to calcite were observed in any samples. Some asymmetry in certain peaks was observed due to the presence of different concentrations of aragonite, vaterite and calcium magnesium carbonate. All samples contained NaCl. NaCl peaks were particularly apparent in sample group 2. Aragonite was detected in all three samples. Possibly, aragonite may have been synthesized by sterilization of microparticle groups in the autoclave.

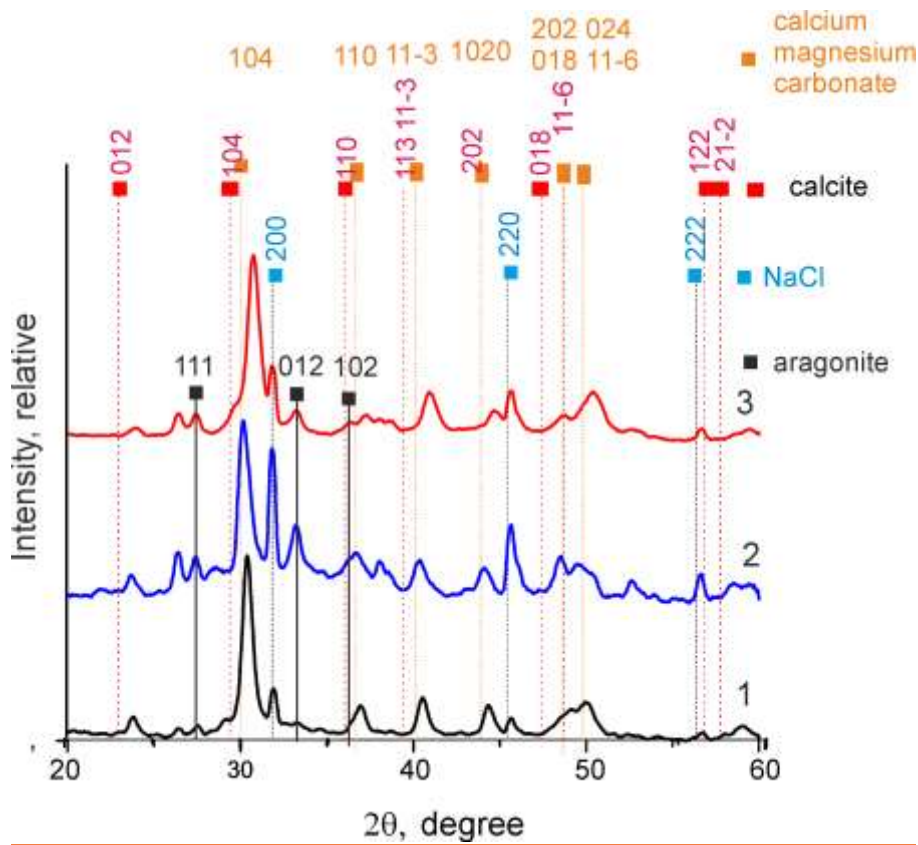


Figure 3 . XRD analysis of microparticle groups 1, 2 and 3.

FTIR analysis (Figure S7) showed that all microparticle groups displayed a prominent band at approximately 1400 cm^{-1} , corresponding to ν_3 antisymmetric stretching of CO_3^{2-} , and bands at approximately 720 cm^{-1} , 870 cm^{-1} and 1090 cm^{-1} , corresponding to ν_4 antisymmetric bending, ν_2 symmetric bending and ν_1 symmetric stretching of CO_3^{2-} , respectively (Andersen and Brecevic, 1991). Microparticle group 3, in contrast to groups 1 and 2, displayed a double band at approximately 870 cm^{-1} . This may indicate the presence of more than one type of carbonate which contains Mg and Ca.

Raman spectra of microparticles are shown in Figure S8. All microparticle groups showed bands at 1094 cm^{-1} and 732 cm^{-1} which are consistent with $\nu^1\text{ CO}_3^{2-}$ symmetric stretching and $\nu^4\text{ CO}_3^{2-}$ in-plane bending, respectively (Bischoff et al., 1985). Bands corresponding to the vibration (L) lattice modes were observed at 300 , 296 and 308 cm^{-1} for microparticle groups 1, 2 and 3, respectively, while bands corresponding to the translation (T) lattice mode were observed at 180 , 167 and 180 cm^{-1} for microparticle groups 1, 2 and 3, respectively (Bischoff et al., 1985). Presumably, these differences are due to differences in the lattice structures caused by the different elemental compositions. Microparticle group 2 displayed bands at 405 and 540 cm^{-1} . The reasons for these remain unclear. The intensity of the signal from microparticle group 3 was lower, which may indicate lower crystallinity. All microparticles also displayed bands at approximately 1450 cm^{-1} , which are characteristic for $\nu^3\text{ CO}_3^{2-}$ antisymmetric stretching (Bischoff et al., 1985). Much weaker bands characteristic for $\nu^3\text{ CO}_3^{2-}$ antisymmetric stretching were observed at 1755 , 1755 and 1781 cm^{-1} for microparticle groups 1, 2 and 3, respectively (Bischoff et al., 1985). Presumably, these differences are due to differences in the lattice structures caused by the different elemental compositions. Microparticle group 2 exhibited a band at approximately 1560 cm^{-1} , the reasons for which are unclear.

TGA results (Figure S9) showed that all microparticle groups underwent decomposition during heating up to 800°C. However, differences were observed between groups. The initial weight loss up to 100°C may be ascribed to removal of loosely bound water. The increases in weight percentage loss were 1.63, 0.97 and 9.42 % for groups 1, 2 and 3, respectively. The particularly marked increase for microparticle group 3 suggests that this group contained more loosely bound water.

The increases in weight percentage loss between 100°C and 500°C were 12.99, 9.50 and 18.67 % for groups 1, 2 and 3, respectively. Groups 1 and 2 displayed a gradual increase in weight percentage loss up to 500°C. This might be due to release of CO₂ which has been reported for amorphous calcium carbonate. (Ihli et al., 2013, Raz et al., 2002). The profile of group 3 was different. A sharper increase in weight percentage loss was seen between 320 and 380°C, which accounted for a 7.66 % weight loss. One can speculate that this could be due to release of water of crystallization, which has been reported for certain magnesium carbonates (Hollingbery and Hull, 2010). All groups displayed a increase in weight percentage loss in the range 650-750°C. The increases in weight percentage loss in this range were 15.78, 19.04 and 16.67 % for groups 1, 2 and 3, respectively. Presumably, these increases in weight percentage loss are connected with the thermal decomposition of the carbonates with emission of CO₂ and formation of metal oxides.

The increases in weight percentage loss at 800°C were 37, 34 and 47 % for groups 1, 2 and 3, respectively. Presumably, the higher increase in weight percentage loss for group 3 is due to the greater mass of crystallization water and loosely bound water removed.

3.2 Cell biological characterization of microparticles formed

amarBlue® viability test results are displayed in Figure 4. The experiment showed the

ability of metabolically active cells to convert the [alamarBlue®](#) reagent into a fluorescent and colorimetric indicator. Cells cultured in the presence of microparticle groups 1 and 2 exhibited a significantly (based on the ANOVA test) lower metabolic activity than those on control tissue culture polystyrene; differences between untreated and treated cells were $51\pm4\%$ and $49\pm12\%$. In contrast, cells in wells with microparticle group 3 achieved almost $95\pm17\%$ activity of the untreated cells.

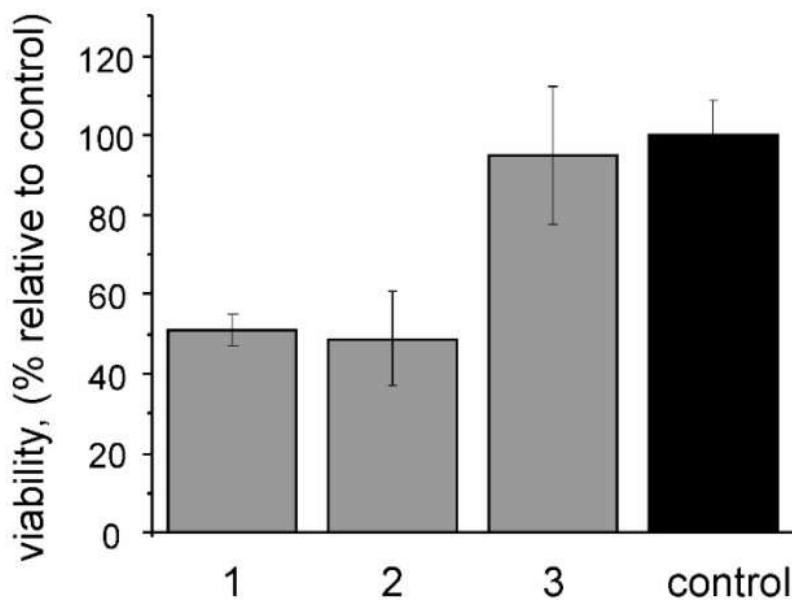


[Figure 4: The cell viability for the microparticles groupes 1, 2, and 3 determined by the alamarBlue® assay](#)

3.3 Physicochemical characterization of hydrogel-microparticle composites, antibacterial testing and cell biological characterization of hydrogel-microparticle composites with MC3T3-E1 osteoblast-like cells

Results of rheometric analysis are shown in Figure S9. In all cases gelation was completed

after 600 s. In the case of composites containing microparticle groups 1 and 3, the storage modulus G' , a measure of sample elasticity, increased markedly during the first 600 s and appeared to reach a plateau value, indicating completion of gelation. In the case of composites containing microparticle group 2, similar gelation kinetics were observed, though the increase in G' was not so marked.

Results of antibacterial testing are presented in Figure 5. No significant differences in CFU number were observed for GG hydrogels without any particles (CTRL GG) and hydrogel-microparticle composites containing group 1 (C1) or group 2 (C2). Hydrogel-microparticle composites containing group 3, which did not contain Zn, were significantly more antibacterial, with >99.99% less bacteria remaining on silicone discs if they were incubated with composites containing microparticle group 3 compared to the control group.

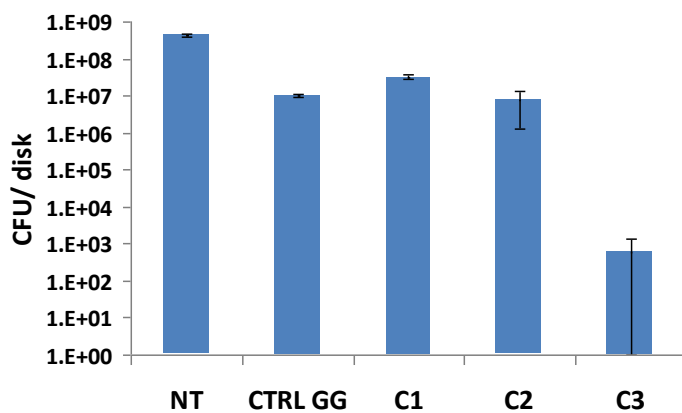


Figure 5. Antibacterial testing of ability of hydrogel-microparticle composites to inhibit growth of MRSA. Error bars show standard deviation, n=3. NT: no composite. CTRL GG: C1, C2, C3: hydrogel-microparticle composites containing microparticle groups 1, 2 and 3, respectively.

Fluorescence microscopy images of MC3T3-E1 cells cultured directly on, under or inside hydrogel-microparticle composites are shown in Figure 6. As the best cytocompatibility was shown by microparticle group 3 and since hydrogel-microparticle composites containing group 3 showed the highest antibacterial activity, culture of MC3T3-E1 cells was performed with composites containing group 3 only. In the qualitative observations, cell viability was found to be comparable in all the applied combinations. Viable cells were observed after both 1 and 7 days, regardless of whether cells were cultured directly on, under or inside composites. A certain number of dead cells were observed in all cases as well. Cells cultured on or inside composites displayed a round morphology, while those cultured under hydrogels exhibited a more stretched morphology.

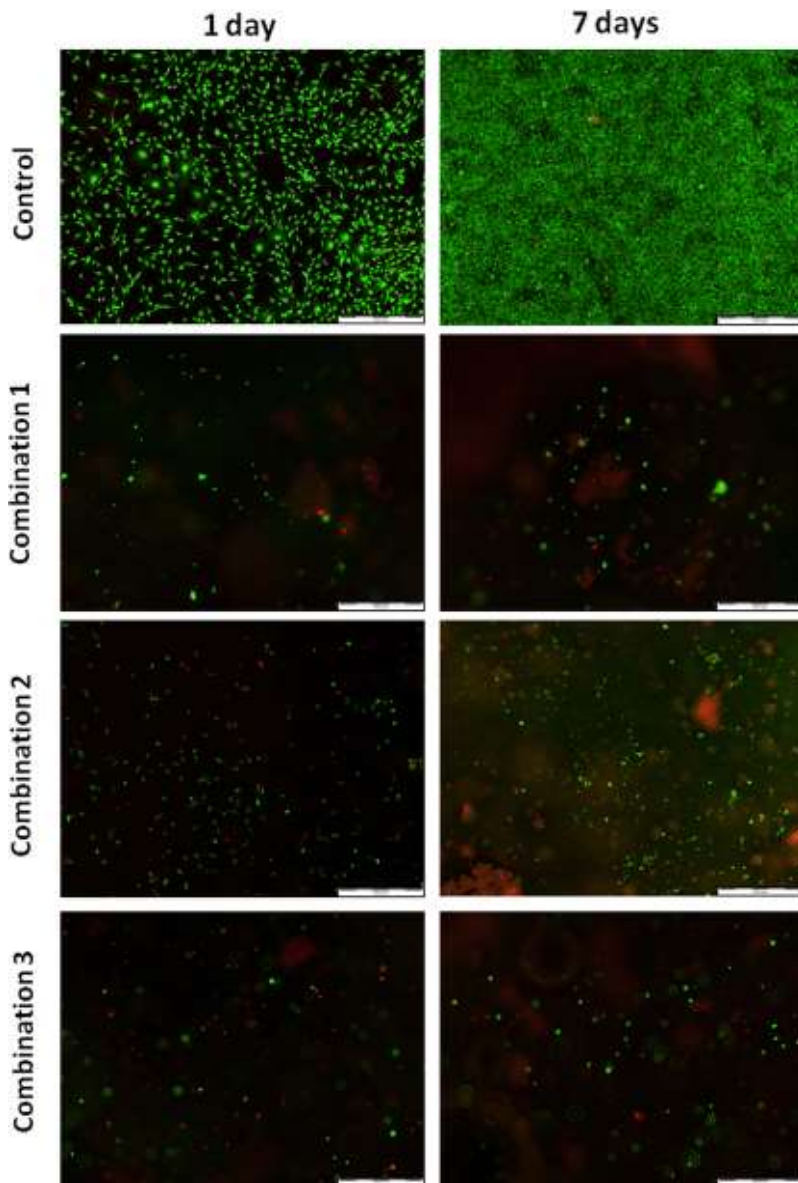


Figure 6. Live/Dead images of [MC3T3-E1](#) cells after 1 day (left column) and 7 days (right column). Top row: Control Second row from top: Combination 1: cells on hydrogel. Third row from top: Combination 2: cells under hydrogel. Bottom row: Combination 3: cells suspended in hydrogel. Scale bar = 500 μm on all images.

4. Discussion

The main goals of the present study were the generation and characterization of carbonate particles with different Ca, Mg and Zn contents and the generation of injectable GG hydrogel-microparticle composites and their characterization.

4.1. Physicochemical and cell biological characterization of microparticles

According to the results of XRF analysis (Table 2), in microparticle groups 1 and 2, more Zn was incorporated than Mg, while in microparticle group 3, more Ca was incorporated than Mg. Presumably, Mg^{2+} ions do not [dissociate from water](#) as quickly as Zn^{2+} than Ca^{2+} , and thus fewer Mg^{2+} ions are incorporated into the crystal structures. Indeed, it is known that Mg^{2+} ions, being more strongly hydrated than Ca^{2+} ions, can bind to the surface of calcite nuclei and hinder further crystal growth (Folk, 1974). Indeed, the TGA results (Figure S7) [suggest](#) the presence of water in microparticle group 3, which contained the most Mg and no Zn. It is unclear from elemental mapping (Figures S4, S5, S6) if Mg is present on the surface or in the interior of particles.

All microparticle groups were heterogeneous and contained particles of different sizes, elemental compositions and crystallinities as demonstrated by SEM (Figure 1), TEM, SEAD and elemental mapping (Figures 2, S4, S5, S6). It appeared that Zn-rich deposits contained smaller crystallites than Ca- and Mg-rich deposits. Since the Zn-rich deposits were “star shaped”, while the Ca- and Mg-rich deposits were irregular in shape, it can be speculated that these were more crystalline. Microparticle group 3, which was Zn-free, displayed a weaker Raman signal intensity (Figure S8), [and contained a larger amount of loosely bound water \(Figure S9\)](#) which may also suggest lower overall crystallinity. [Increasing the amount of Mg has been known to reduce the crystallinity of \$CaCO_3\$ and calcium phosphate \(Douglas et al.,](#)

2016b), presumably due to binding of Mg^{2+} to the surface of amorphous phases, leading to the stabilization of the amorphous phase (Folk, 1974, Neuman and Mulryan, 1971). The reasons for the heterogeneity of particle sizes remain unclear. XRD analysis (Figure 3) revealed a certain overall crystallinity of all microparticle groups. XRD analysis also provided further evidence for the heterogeneity of microparticle groups, as NaCl and aragonite were detected in all groups. XRD also revealed the presence of crystalline phases which are difficult to identify.

Cytotoxicity testing of microparticles (Figure 4) revealed that microparticle groups containing Zn, i.e. 1 and 2, were cytotoxic. In contrast, microparticle group 3, which contained no Zn, did not display significant cytotoxicity. One explanation may be the release of Zn from groups 1 and 2, as Zn has been reported to be cytotoxic in solution above 400 μ M (Brauer et al., 2011). Despite the differences in Zn content between groups 1 and 2 (Table 2), no marked differences in cytotoxicity between these two groups were observed. Alternatively, the poorer viability of cells cultured in the presence of microparticle groups 1 and 2 might be explained by changes in the pH of the cell culture medium due to Zn, leading to a loss of cellular metabolic activity. The fate of microparticles remains unclear.

4.2 Hydrogel-microparticle composites: physicochemical characterization, antibacterial testing and cell biological characterization

All microparticle groups induced gelation of GG (Figure S10). It is known that divalent ions, including Mg^{2+} , Ca^{2+} and Zn^{2+} , can crosslink GG (Douglas et al., 2014b, Grasdalen and Smidsrod, 1987). Thus, it can be assumed that ion release for all three groups is sufficient to induce GG hydrogel formation. The fact that gelation time was less than 600 s, i.e. 10 minutes, appears to be compatible with clinical surgical procedures, suggesting that the composites can be used as injectable materials.

Composites containing microparticle group 3, which contained no Zn, displayed higher antibacterial activity (Figure 5). This result was unexpected, as Zn is known for its antibacterial activity (Douglas et al., 2014a). It can be speculated that the “star shaped” Zn-rich deposits are more crystalline than the Ca- and Mg-rich deposits (Figures 2, 4, S4, S5, S6), and thus less Zn is released than Ca and Mg. Possibly, the ion release from composites containing microparticle group 3 is higher, which may lead to pH changes in the bacterial culture medium which are unfavorable for bacterial growth. [It is known that pH increases are detrimental to bacterial growth \(Gubler et al., 2008\)](#). It is possible that the ion concentrations in the medium as a result of ion release are inherently unfavorable for bacterial growth, however further experiments would be needed to confirm this. [Antibacterial activity has been reported for CaCO₃ materials containing Mg; CO₃/MgO produced by pyrolysis of poly\(vinyl alcohol\)-dolomite exhibited bacteriocidal activity against *S. aureus* and *E. coli* \(Yamamoto et al., 2008\)](#). The authors suggested a rise and pH and generation of active oxygen species such as super-oxide anions as possible explanations for the antibacterial activity. [Antibacterial activity was also reported for heated dolomite slurry \(Sawai et al., 2005\)](#). The authors [attributed the antibacterial activity to the generation of CaO and MgO upon heating](#). [The number of samples in each group was 3; this should be taken into account when interpreting the data](#).

Cytotoxicity testing of hydrogel-microparticle composites containing microparticle group 3 (Figures 6) revealed that the proportion of viable to dead cells appeared roughly similar, regardless of the seeding technique applied (in, under or above composites). [Generally, for the osteoblast-like cells, culture systems which allow cell attachment and spreading are more favorable. It was observed that both cells in the control \(routine observation in culture dish\) and the cells located under the material \(Combination 2\), were elongated, which might have been expected as they are in direct contact with tissue culture polystyrene. However, although](#)

the population of living cells was visibly highest in the control, the elongated morphology of the cells located under the material was not accompanied by a higher cell viability as compared to the other hydrogel-based systems. As expected, both cells cultured on the surface of the hydrogel (Combination 1) and those observed in the suspension (Combination 3), were round in shape. However, their viability was not diminished as compared to the systems which allow cell spreading (control, Combination 2). From the point of view of the main goal of this study, the observation of cell fate in suspension (Combination 3), which mimics a potentially injectable system, is of particular interest. It was shown that even though the cells suspended in the hydrogel (Combination 3) did not have opportunity to become flattened, the population of living cells was similar to other combinations up to day 7. This finding seems to be encouraging from the point of view of the planned use of the injectable system in which cells are to be delivered in the form of a suspension in the hydrogel. For further development of the system, more precise characterization of the behavior of the cells suspended in the investigated composite is required.

5. Conclusions

This study proves the principle that one can create bi- and tri-elemental microparticles to induce the gelation of an anionic polymer (GG) to create injectable hydrogel-microparticle composites. Zn and Ca were incorporated into microparticle preparations to a greater extent than Mg. Microparticle groups were heterogeneous and contained microparticles of differing shape and elemental composition. Zn-rich microparticles were “star shaped” and appeared to consist of small crystallites, while Zn-poor, Ca- and Mg-rich microparticles were irregular in shape and appeared to contain larger crystallites. Zn-free microparticle groups exhibited the best cytocompatibility and, unexpectedly, Zn-free composites showed the highest antibacterial activity. These results pave the way for applications of this composite as an injectable

biomaterial.

6. Acknowledgement

T.E.L.D., B.V.P. and A.G.S. acknowledge the Research Foundation Flanders (FWO) for support in the framework of a postdoctoral fellowship. Tom Planckaert, Danny Vandeput, and Joanna Aernoudt are thanked for excellent technical assistance. Prof. Kevin Braeckmans and Dr. Bart Lucas are thanked for enabling rheometrical measurements to be performed. A.G.S. also acknowledges the support of BOF UGent. The ERA-Net Rus Plus project “Fabrication and investigation of new hybrid scaffolds with the controlled porous hierarchy for bone tissue engineering” (Intelbiocomp) is thanked for support. T.E.L.D., K.W. and M.L-S. acknowledge the FWO and Polish Academy of Sciences (PAN) for support in the framework of the joint project “Biomimetic three-phase biomaterials for regeneration of mineralized and unmineralized tissues”.

7. Conflict of Interest, Ethical Approval, Original Publication and Author Contribution Statements

The authors have no conflict of interest. No ethical approval was required for this study. No part of this work has been previously published or submitted for publication elsewhere. The authors made the following contributions to the paper: Timothy E.L. Douglas conceived, designed, planned and coordinated the study, interpreted the data and wrote the majority of the manuscript. Katarzyna Sobczyk produced the microparticles and hydrogel-microparticle composites, performed rheometry (Figure S10) and together with Agata Łapa, Katarzyna Reczyńska and Krzysztof Pietryga, devised the methodology of microparticle and hydrogel-microparticle composites (Figure S1) and performed preliminary experiments, EDS (Figure S2) and laser diffraction (Figure S3). Katarzyna Włodarczyk, Heidi A. Declercq and

Małgorzata Lewandowska-Szumiel performed cell biological characterization of hydrogel-microparticle composites (Figure 6). Gilles Brackman and Tom Coenye performed antibacterial testing (Figure 5). Irina Vidiyasheva performed cell biological characterization of microparticles (Figure 4). David Schaubroeck performed SEM analysis (Figure 1). Vitaliy Bliznuk performed TEM and SAED analysis and EDS-based elemental mapping (Figures 2, S4, S5, S6). Pascal Van Der Voort performed XRF analysis (Table 2) [and XRD measurements \(Figure 3\)](#). Jan Van den Bulcke and Joris Van Acker performed TGA (Figure S9). Sangram Keshari Samal performed FTIR analysis (Figure S7). Dmitry Khalenkow performed Raman analysis (Figure S8). Bogdan V. Parakhonskiy [conducted in-depth analysis of XRD measurements \(Figure 3\) and](#) assisted greatly with analysis and presentation of results. Elżbieta Pamuła co-coordinated the study, co-performed extensive preliminary studies, instructed K. Sobczyk, A. Łapa, K. Reczynska and K. Pietryga in sample preparation and provided significant logistical help. Andre G. Skirtach co-coordinated the study and provided significant logistical help. All authors contributed to the interpretation of the results and the improvement of the discussion.

8. References

- ANDERSEN, F. A. & BRECEVIC, L. (1991) Infrared-Spectra of Amorphous and Crystalline Calcium-Carbonate. *Acta Chem Scand*, 45, 1018-1024.
- BISCHOFF, W. D., SHARMA, S. K. & MACKENZIE, F. T. (1985) Carbonate Ion Disorder in Synthetic and Biogenic Magnesian Calcites - a Raman Spectral Study. *American Mineralogist*, 70, 581-589.
- BRAUER, D. S., GENTLEMAN, E., FARRAR, D. F., STEVENS, M. M. & HILL, R. G. (2011) Benefits and drawbacks of zinc in glass ionomer bone cements. *Biomed Mater*, 6, 045007.
- CHAN, L. W., LEE, H. Y. & HENG, P. W. S. (2002) Production of alginate microspheres by internal gelation using an emulsification method. *International Journal of Pharmaceutics*, 242, 259-262.
- DONATAN, S., YASHCHENOK, A., KHAN, N., PARAKHONSKIY, B., COCQUYT, M., PINCHASIK, B. E., KHALENKOW, D., MOHWALD, H., KONRAD, M. & SKIRTACH, A. (2016) Loading Capacity versus Enzyme Activity in Anisotropic and Spherical Calcium Carbonate Microparticles. *Acs Applied Materials & Interfaces*, 8, 14284-14292.
- DOUGLAS, T., WLODARCZYK, M., PAMULA, E., DECLERCQ, H., DE MULDER, E., BUCKO, M., BALCAEN, L., VANHAECKE, F., CORNELISSEN, R., DUBRUEL, P., JANSSEN, J. & LEEUWENBURGH, S. (2014a) Enzymatic mineralization of gellan gum hydrogel for bone tissue-engineering applications and its enhancement by polydopamine. *J Tissue Eng Regen*

Med, 8, 906–918.

- DOUGLAS, T. E., DOKUPIL, A., RECYNSKA, K., BRACKMAN, G., KROK-BORKOWICZ, M., KEPPLER, J. K., BOZIC, M., VAN DER VOORT, P., PIETRYGA, K., SAMAL, S. K., BALCAEN, L., VAN DEN BULCKE, J., VAN ACKER, J., VANHAECKE, F., SCHWARZ, K., COENYE, T. & PAMULA, E. (2016a) Enrichment of enzymatically mineralized gellan gum hydrogels with phlorotannin-rich *Ecklonia cava* extract Seanol((R)) to endow antibacterial properties and promote mineralization. *Biomed Mater*, 11, 045015.
- DOUGLAS, T. E., LAPA, A., RECYNSKA, K., KROK-BORKOWICZ, M., PIETRYGA, K., SAMAL, S. K., DECLERCQ, H. A., SCHAUBROECK, D., BOONE, M., VAN DER VOORT, P., DE SCHAMPHELAERE, K., STEVENS, C. V., BLIZNUK, V., BALCAEN, L., PARAKHONSKIY, B. V., VANHAECKE, F., CNUUDE, V., PAMULA, E. & SKIRTACH, A. G. (2016b) Novel injectable, self-gelling hydrogel-microparticle composites for bone regeneration consisting of gellan gum and calcium and magnesium carbonate microparticles. *Biomed Mater*, 11, 065011.
- DOUGLAS, T. E., PIWOWARCZYK, W., PAMULA, E., LISKOVA, J., SCHAUBROECK, D., LEEUWENBURGH, S. C., BRACKMAN, G., BALCAEN, L., DETSCH, R., DECLERCQ, H., CHOLEWA-KOWALSKA, K., DOKUPIL, A., CUIJPERS, V. M., VANHAECKE, F., CORNELISSEN, R., COENYE, T., BOCCACCINI, A. R. & DUBRUEL, P. (2014b) Injectable self-gelling composites for bone tissue engineering based on gellan gum hydrogel enriched with different bioglasses. *Biomed Mater*, 9, 045014.
- DOUGLAS, T. E. L., KRAWCZYK, G., PAMULA, E., DECLERCQ, H., SCHAUBROECK, D., BUCKO, M. M., BALCAEN, L., VAN DER VOORT, P., BLIZNUK, V., VAN DER VREKEN, N. M., VANHAECKE, F., DASH, M., DETSCH, R., BOCCACCINI, A. R., CORNELISSEN, R. & DUBRUEL, P. (2014c) Generation of composites for bone tissue engineering applications consisting of gellan gum hydrogels mineralized with calcium and magnesium phosphate phases by enzymatic means. *J Tissue Eng Regen Med*.
- DOUGLAS, T. E. L., PILARZ, M., LOPEZ-HEREDIA, M., BRACKMAN, G., SCHAUBROECK, D., BALCAEN, L., BLIZNUK, V., DUBRUEL, P., KNABE-DUCHEYNE, C., VANHAECKE, F., COENYE, T. & PAMULA, E. (2015) Composites of gellan gum hydrogel enzymatically mineralized with calcium–zinc phosphate for bone regeneration with antibacterial activity. *J Tiss Eng Regen Med*, Epub 15.7.2015.
- FOLK, R. L. (1974) Natural-History of Crystalline Calcium-Carbonate - Effect of Magnesium Content and Salinity. *Journal of Sedimentary Petrology*, 44, 40-53.
- GKIONI, K., LEEUWENBURGH, S. C., DOUGLAS, T. E., MIKOS, A. G. & JANSEN, J. A. (2010) Mineralization of hydrogels for bone regeneration. *Tissue Eng Part B Rev*, 16, 577-85.
- GORODZHA, S., DOUGLAS, T. E., SAMAL, S. K., DETSCH, R., CHOLEWA-KOWALSKA, K., BRAECKMANS, K., BOCCACCINI, A. R., SKIRTACH, A. G., WEINHARDT, V., BAUMBACH, T., SURMENEVA, M. A. & SURMENEV, R. A. (2016) High-resolution synchrotron X-Ray analysis of bioglass-enriched hydrogels. *J Biomed Mater Res A*.
- GRASDALEN, H. & SMIDSDROD, O. (1987) Gelation of Gellan Gum. *Carbohydrate Polymers* 7, 371-393.
- GUBLER, M., BRUNNER, T. J., ZEHNDER, M., WALTIMO, T., SENER, B. & STARK, W. J. (2008) Do bioactive glasses convey a disinfecting mechanism beyond a mere increase in pH? *International Endodontic Journal*, 41, 670-678.
- HOLLINGBERY, L. A. & HULL, T. R. (2010) The thermal decomposition of huntite and hydromagnesite-A review. *Thermochimica Acta*, 509, 1-11.
- IHLI, J., KULAK, A. N. & MELDRUM, F. C. (2013) Freeze-drying yields stable and pure amorphous calcium carbonate (ACC). *Chemical Communications*, 49, 3134-3136.
- JAROSCH, D. & HEGER, G. (1986) Neutron-Diffraction Refinement of the Crystal-Structure of Aragonite. *Tschermaks Mineralogische Und Petrographische Mitteilungen*, 35, 127-131.
- KUO, C. K. & MA, P. X. (2001) Ionically crosslinked alginate hydrogels as scaffolds for tissue engineering: part 1. Structure, gelation rate and mechanical properties. *Biomaterials*, 22, 511-21.
- LANDI, E., TAMPIERI, A., MATTIOLI-BELMONTE, M., CELOTTI, G., SANDRI, M., GIGANTE, A. & FAVA, P. (2006) Biomimetic Mg- and Mg, CO₃-substituted hydroxyapatites: synthesis,

- characterization and in vitro behaviour. *J Eur Ceram Soc*, 26, 2593-601.
- LE BAIL, A., OUHENIA, S. & CHATEIGNER, D. (2011) Microtwinning hypothesis for a more ordered vaterite model. *Powder Diffr*, 26, 16-21.
- MOREIRA, H. R., MUNARIN, F., GENTILINI, R., VISAI, L., GRANJA, P. L., TANZI, M. C. & PETRINI, P. (2014) Injectable pectin hydrogels produced by internal gelation: pH dependence of gelling and rheological properties. *Carbohydrate Polymers*, 103, 339-347.
- NEUMAN, W. F. & MULRYAN, B. J. (1971) Synthetic hydroxyapatite crystals. IV. Magnesium incorporation. *Calcif Tissue Res*, 7, 133-8.
- PARAKHONSKIY, B. V., FOSS, C., CARLETTI, E., FEDEL, M., HAASE, A., MOTTA, A., MIGLIARESI, C. & ANTOLINI, R. (2013) Tailored intracellular delivery via a crystal phase transition in 400 nm vaterite particles. *Biomaterials Science*, 1, 1273-1281.
- RAZ, S., TESTENIERE, O., HECKER, A., WEINER, S. & LUQUET, G. (2002) Stable amorphous calcium carbonate is the main component of the calcium storage structures of the crustacean *Orchestia cavimana*. *Biological Bulletin*, 203, 269-274.
- REEDER, R. J. & MARKGRAF, S. A. (1986) High-Temperature Crystal-Chemistry of Dolomite. *American Mineralogist*, 71, 795-804.
- SAVELYEVA, M. S., ABALYMOV, A. A., LYUBUN, G. P., VIDYASHEVA, I. V., YASHCHENOK, A. M., DOUGLAS, T. E. L., GORIN, D. A. & PARAKHONSKIY, B. V. (2017) Vaterite coatings on electrospun polymeric fibers for biomedical applications. *Journal of Biomedical Materials Research Part A*, 105, 94-103.
- SAWAI, J., HIMIZU, K. & YAMAMOTO, O. (2005) Kinetics of bacterial death by heated dolomite powder slurry. *Soil Biology & Biochemistry*, 37, 1484-1489.
- SITEPU, H. (2009) Texture and Structural Refinement Using Neutron Diffraction Data from Molybdite (MoO₃) and Calcite (CaCO₃) Powders and a Ni-Rich Ni_{50.7}Ti_{49.30} Alloy. *Powder Diffr*, 24, 315-326.
- STRELTSOV, V. A., TSIRELSON, V. G., OZEROV, R. P. & GOLOVANOV, O. A. (1987) Electronic and Thermal Properties of Ions in CaF₂: Regularized Least Squares Treatment. *Kristallografiya*, 33, 90-97.
- SVENSKAYA, Y., PARAKHONSKIY, B., HAASE, A., ATKIN, V., LUKYANETS, E., GORIN, D. & ANTOLINI, R. (2013) Anticancer drug delivery system based on calcium carbonate particles loaded with a photosensitizer. *Biophys Chem*, 182, 11-5.
- SVENSKAYA, Y. I., PAVLOV, A. M., GORIN, D. A., GOULD, D. J., PARAKHONSKIY, B. V. & SUKHORUKOV, G. B. (2016) Photodynamic therapy platform based on localized delivery of photosensitizer by vaterite submicron particles. *Colloids and Surfaces B-Biointerfaces*, 146, 171-179.
- THIAN, E. S., KONISHI, T., KAWANOBE, Y., LIM, P. N., CHOONG, C., HO, B. & AIZAWA, M. (2013) Zinc-substituted hydroxyapatite: a biomaterial with enhanced bioactivity and antibacterial properties. *J Mater Sci Mater Med*, 24, 437-45.
- VIATEAU, V., MANASSERO, M., SENSEBE, L., LANGONNE, A., MARCHAT, D., LOGEART-AVRAMOGLU, D., PETITE, H. & BENSIDHOUM, M. (2013) Comparative study of the osteogenic ability of four different ceramic constructs in an ectopic large animal model. *J Tissue Eng Regen Med*.
- YAMAMOTO, O., OHIRA, T., MOHAN, D. J., FUKUDA, M., OZKAL, B., SAWAI, J. & NAKASAWA, Z. (2008) Antibacterial characteristics of carbon-coated CaCO₃/MSO powder led by the pyrolysis of poly(vinyl alcohol) -dolomite mixture. *TANSO*, 232, 77-81.
- ZHAO, S. F., JIANG, Q. H., PEEL, S., WANG, X. X. & HE, F. M. (2012) Effects of magnesium-substituted nanohydroxyapatite coating on implant osseointegration. *Clin Oral Implants Res*.